Characteristics of Nuclear Radiation Shielding using Natural Bentonitic Shale

Samah Abdullah Abd El-Azeem
Physics Department, College of Sciences and Humanities, Prince Sattam Bin Abdulaziz University, Al-Kharj 11942, Saudi Arabia | Physics Department, Faculty of Women for Arts, Science and Education, Ain Shams University, Cairo 11757, Egypt
drsamah2020.sa@gmail.com (corresponding author)

Nareman M. Harpy
Nuclear Materials Authority, P.O. Box 530, El-Maadi, Cairo 11728, Egypt
karem_249@hotmail.com

Howaida Mansour
Physics Department, Faculty of Women for Arts, Science and Education, Ain Shams University, Cairo 11757, Egypt
hoyda_mans@yahoo.com

Received: 12 July 2024 | Revised: 1 August 2024 | Accepted: 5 August 2024

 DOI: https://doi.org/10.48084/etasr.8374

ABSTRACT

With the wide use of radioactive materials, it is important to look for locally available and inexpensive materials to serve as efficient absorbers, suitable for shielding against radiation hazards. Due to its widespread availability and affordability, natural bentonitic shale is a viable option for use as a nuclear shielding material. In this study, natural bentonitic samples were cut into cylindrical pellets of varying thicknesses. The chemical composition of the natural bentonitic shale samples was determined through the use of X-Ray Fluorescence (XRF) spectroscopy. The linear and mass attenuation coefficients of bentonitic samples were evaluated using a NaI(Tl) scintillation detector at 662 keV energy of ^{137}Cs, as well as at 1,173 keV and 1,332 keV energies of ^{60}Co, gamma-ray sources. The experimental results indicated that bentonitic samples B3 and M2 exhibited superior shielding parameters compared to other bentonitic samples, attributable to their elevated densities. These two samples are distinguished by a high CaO content and a low Al_2O_3 content. Furthermore, the Half Value Layer (HVL), Tenth Value Layer (TVL), and mean free path thicknesses were calculated at these energies using linear attenuation coefficients. The theoretical mass attenuation coefficient, calculated with the assistance of the XCOM program and experimental estimates, was found to be in good agreement with the theoretical value.

Keywords-radiation shielding; attenuation coefficients; natural clay; bentonitic shale

I. INTRODUCTION

The penetration of solid objects by gamma rays, which are ionizing radiation with very short wavelengths, depends on the energy of the radiation. Additionally, gamma radiation can readily penetrate the body's tissues, posing a significant risk to human health, both internally and externally. Gamma radiation causes DNA damage and cell death in the human body through deterministic and stochastic biological effects [1-3]. The necessity for shielding protection arises from a multitude of industrial applications, including reactors, storage of spent fuel, radiology, nuclear medicine, and others [4]. In order to safeguard against the potentially deleterious consequences of high-dose gamma radiation exposure, radiation shielding materials have been developed [5-7]. Concretes and lead were initially widely utilized as radiation shielding materials due to their effective shielding capabilities, low cost, high density, great mass attenuation, and simple maintenance. However, due to limitations, such as poor mechanical qualities, low chemical resistance, toxicity, and health concerns, they are no longer suitable for use in various nuclear technology applications [2, 8-10]. Concrete, which is known for its inert properties, plays a critical role in nuclear and radioactive waste storage, providing a robust barrier against radiation. Recently, blended concrete made up of composite materials, namely barite or magnetite, has been employed as radiation shielding concrete [11].

In order to gain a deeper understanding of the shielding properties of different materials, further research is required. Due to their low cost and abundance, natural rocks and minerals have been the subject of considerable interest from the research community [12-14]. Mineral ores can be employed as

gamma ray shielding agents due to their composition of a range of light and heavy elements, including carbon (C), potassium (K), sulfur (S), phosphorus (P), calcium (Ca), magnesium (Mg), and sodium (Na), among others [15, 16]. Natural bentonite is a mineral resource comprising a range of oxides that can function as a gamma ray shield. Bentonite is a soft, porous rock consisting mainly of the clay mineral montmorillonite, which has the property of expanding its lattice with a general formula of $R{\times}0.33{\times}Al_2Si_4O_{10}(OH)_2{\times}n$H2O, where R includes one or more of the cations Na+, K+, Mg_2+, Ca_2+ and possibly others [17,18]. The minerals are distinguished by a three-layer crystal lattice comprising one sheet of aluminum and hydroxyl between two sheets of silicon and oxygen. The material in question displays a notable swelling upon wetting and a corresponding shrinking upon drying, which can be attributed to the introduction of considerable interlayer water along the *C*-axis direction. Montmorillonite minerals are typically derived from the alteration of ferromagnesian minerals, calcic feldspars, and volcanic ashes, which represent the primary constituent of bentonite and are commonly found in soils and sedimentary rocks [19, 20]. The objective of the present study is to identify more efficient gamma ray shielding materials that are dependable in radiation research. The linear and mass attenuation coefficients of radiation were investigated at energies of 662, 1,173, and 1,332 keV for a series of samples. Other parameters, including the half-value layer, tenth-value layer, and mean free path, were subsequently estimated using the aforementioned determined values. The outcomes of the μ/ρ ratio have been contrasted with the theoretical results yielded by the WinXCOM program.

II. THEORETICAL STUDY

The Lambert-Beer law, which explains the transmission of a narrow beam photon through a thin absorbing material, can be used to compute the linear attenuation coefficient as follows:

$$I(x) = I_0\, e^{-\mu x} \quad (1)$$

where, I_0 is the original intensity of the beam, $I(x)$ is the transmitted intensity through an absorber to thickness x, and μ is the linear absorption coefficient for the absorbing material. The mass attenuation coefficient (μ_m) for photons is given by:

$$\mu_m = \ln\left(\frac{I_0}{I}\right)/\rho x \quad (2)$$

where ρ is the shield material's density and (μ/ρ) is the mass attenuation coefficient which quantifies the probability of interaction between light photons and matter per unit mass per unit area [21].

According to the mixing rule, the total mass attenuation coefficients of compounds or mixtures are computed. Equation (3) derives the theoretical mass attenuation coefficients received from the XCOM program at various energies [22, 23]:

$$\mu_m = \sum w_i \mu_i \quad (3)$$

where μ_i denotes the mass attenuation coefficient of the i element and w_i is the mass proportion of the element i in the entire mixture [24]. Equation (4) is used to calculate the standard deviation between experimental and theoretical mass attenuation coefficient values that were calculated deploying the XCOM program:

$$Deviation\ (\%) = \frac{\mu_m(theoretical) - \mu_m(experimental)}{\mu_m(theoretical)} \times 100 \quad (4)$$

Two parameters, the HVL and the TVL, can be employed to ascertain the effective thickness of the shielding material. This can be accomplished through the use of (5) and (6), wherein μ represents the linear attenuation coefficient. HVL and TVL, in turn, refer to the thicknesses of the shielding materials that result in a reduction of the initial intensity of gamma rays to half and one-tenth of their original values, respectively [25]:

$$HVL = \frac{\ln(2)}{\mu} \quad (5)$$

$$TVL = \frac{\ln(10)}{\mu} \quad (6)$$

The Mean Free Path (MFP) is defined as the average distance between two subsequent photon contacts in an absorber material. It can be calculated using (7), where μ is the linear attenuation coefficient [20, 26]:

$$mfp = \frac{1}{\mu} \quad (7)$$

III. MATERIALS AND METHODS

The sedimentary rock samples were collected from three distinct geologic periods and two disparate localities. The initial group, designated B1, B2, B3, M1, M2, and M3, was retrieved from the southwestern region of Sinai, Egypt. Out of these samples, three (B1, B2, and B3) are associated with the Maastrichtian period (approximately 70 million years ago), while the remaining three (M1, M2, and M3) correlate with the Paleocene period. The second group, Q1, Q2, Q3, and Q4, comprises two samples collected from the north El Qattamiya asphaltic road (Q1 and Q2) and two samples collected from the south of the road in Cairo, Egypt (Q3 and Q4). These samples are related to the upper Eocene and are detailed in Table I.

TABLE I. SAMPLE LOCATIONS

Samples no.	System	Series	Time
B1	Cretaceous	Upper	≅ 70Ma
B2	Cretaceous	Upper	≅ 70Ma
B3	Cretaceous	Upper	≅ 70Ma
M1	Paleocene	Lower	≅ 65Ma
M2	Paleocene	Upper	≅ 55Ma
M3	Paleocene	Upper	≅ 55Ma
Q1	Eocene	Upper	≅ 40Ma
Q2	Eocene	Upper	≅ 40Ma
Q3	Eocene	Upper	≅ 40Ma
Q4	Eocene	Upper	≅ 40Ma

The bentonitic shale was crushed into small particles using a hammermill. The material was then divided into cylindrical pellets of varying thicknesses, as shown in Figure 1. The attenuation coefficients of each sample were measured for gamma rays of 662 keV energy of ^{137}Cs, 1,173 keV and 1,332 keV energy of ^{60}Co sources using a gamma ray spectrometer with a 3″x3″ NaI(Tl) scintillation detector. The detector is protected from induced X-rays by a cylindrical copper barrier

and a chamber of lead bricks against ambient radiation. The detector is connected to Nuclear Enterprises' primary shaping amplifier, as well as a high-voltage power supply with a digital display of the applied voltage. Furthermore, the detector is connected to a Nuclease PCA-8000 computer-based 8192-channel analyzer with color graphical spectra display and advanced technical operation features. The narrow beam geometry with a lead collimator was employed for the absorption of gamma radiation in the materials under investigation, as evidenced in Figure 2.

Fig. 1. Different thicknesses of the natural bentonitic shale.

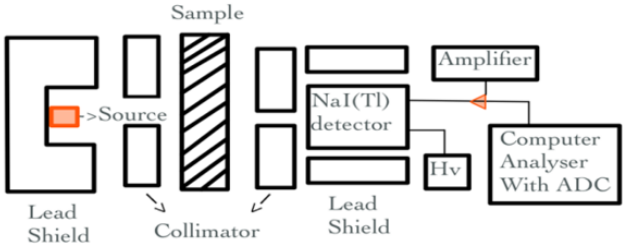

Fig. 2. Schematic diagram of the experimental set-up.

IV. RESULTS AND DISCUSSION

Bentonite has been the subject of investigation as a potential clay material for the manufacture of bricks with enhanced radiation attenuation properties in comparison to those of traditional bricks [27]. The XRF technique was deployed for the characterization of the natural bentonitic shale. Bentonitic shale is a mixture of elements that can be used as a composite gamma ray shielding material, given its composition of a range of clay oxide minerals. Table II presents a chemical composition examination of natural bentonitic shale. Sample B3 bentonitic shale exhibits the highest Loss of Ignition (L.O.I.) at 36.05% due to the presence of water and organic materials. Given that it is composed of volcanic ash deposits, natural bentonite is nanoscale in nature. Volcanic ashes are regarded as naturally occurring nanomaterials, which are defined as materials that are nanometer or smaller in size [28, 29]. The nanoscale dimensions of nanomaterials can result in differences from materials with similar physical or chemical properties. The most significant feature of these materials is their high surface-to-volume ratio, which is a consequence of a number of intrinsic qualities. Research indicates that nanoscale particles may offer enhanced protection against ionizing radiation. It was demonstrated that the shielding properties of nano tin oxide (II) composites are more effective than those of micro tin oxide (II) composites against gamma rays [30].

TABLE II. THE CHEMICAL COMPOSITION OF NATURAL BENTONITIC SHALE

Natural bentonitic samples	**Oxides (%)**													
	SiO_2	Al_2O_3	P_2O_5	TiO_2	Fe_2O_3	CaO	MgO	Na_2O	K_2O	L.O.I (110)	L.O.I (550)	L.O.I (1,000)	Total L.O.I	Total
B1	31.70	10.46	0.26	0.28	2.29	20.72	2.15	1.04	0.95	5.88	3.35	20.92	30.15	100
B2	34.46	10.2	0.25	0.28	2.54	14	4.30	0.9	1.1	6.88	4.36	20.73	31.97	100
B3	24.24	3.57	0.36	0.16	0.90	31.51	2.58	0.21	0.42	1.62	1.61	32.82	36.05	100
M1	58.22	24.74	0.05	0.69	5.40	1.96	1.51	0.21	1.1	2.00	2.49	1.63	6.12	100
M2	30.87	6.63	0.43	0.22	1.55	22.86	2.15	0.79	0.66	6.36	8.88	18.59	33.83	99.99
M3	34.08	8.67	0.56	0.19	1.9	22.51	1.08	0.64	0.81	5.35	7.86	16.35	29.56	100
Q1	34.10	7.14	0.28	0.33	2.13	18.46	7.31	2.69	0.93	2.18	7.11	17.33	26.62	99.99
Q2	33.63	22.7	0.01	0.64	6.00	1.12	0.86	14.97	0.89	8.54	6.14	4.50	19.18	100
Q3	48.97	10.97	0.16	0.36	3.30	7.84	2.58	1.29	0.97	5.09	7.52	10.96	23.57	100.01
Q4	45.90	23.95	0.04	0.80	6.10	1.68	0.86	1.26	1.52	9.00	5.39	3.50	17.89	100

A. Linear Attenuation Coefficient

Table III depicts the observed gamma photons from ^{137}Cs to ^{60}Co point sources with bentonitic absorber material at varying thicknesses and energies. The linear attenuation coefficient μ of the absorber may be calculated for γ-rays with an appropriate energy from the linear graph of the absorber's thickness versus ln (*Io/I*), as portrayed in Figure 3. The slope of the line represents the attenuation coefficient. It is evident that as the thickness of the bentonitic shale was augmented for a range of energies, the attenuation of gamma rays also increased. Figure 4 provides a detailed explanation of the fluctuations in the linear attenuation coefficients observed for all bentonitic samples as a function of incident photon energy. As the photon energy increases, the linear attenuation coefficient exhibits a corresponding decrease. The linear attenuation of bentonitic clay is dependent upon the photon energy, as a result of the differing photon absorption mechanisms, including photoelectric at low energy, Compton scattering at low and mid-energy levels, and pair production at high energy (above 1,022 keV).

As it can be seen in Tables IV, V, and VI, samples B3 and M2 exhibit the highest values of attenuation coefficients (0.167 cm^{-1} and 0.171 cm^{-1} at 661.66 keV, 0.1279 cm^{-1} and 0.1296 cm^{-1} at 1,173.47 keV, and 0.1195 cm^{-1} at 1,332.51 keV), which are significantly higher than those of the other samples. The highest values of attenuation coefficients (1,216 cm^{-1} at

1,332.51 keV) for all photon energy are observed when comparing these samples to other natural bentonitic samples. This is due to the fact that they have the highest density (2.17 g/cm^3 and 2.2 g/cm^3, respectively) of the examined bentonitic samples. As evidenced in Table IV, the mean linear attenuation coefficients (μ) for the M1, M2, and M3 samples from the Paleocene period are the highest, with μ values of 0.167 cm^{-1}, 0.125 cm^{-1}, and 0.1173 cm^{-1} at 661.66 keV, 1,173.47 keV, and 1,332.51 keV, respectively. In contrast, the bentonitic samples from the Eocene period exhibit the lowest μ. Furthermore, a comparison of the chemical composition results in Table II for B3 and M2 with those from the same period revealed that they contained the lowest concentrations of SiO_2, Al_2O_3, Fe_2O_3, and K_2O and the highest concentrations of total L.O.I.

TABLE III. GAMMA PHOTON MEASUREMENTS WITH DIFFERENT BENTONITIC ABSORBER MATERIALS AT VARIOUS THICKNESSES AND ENERGIES LN(I_0/I)

Samples code	Thickness (cm)	Energy (keV)		
		661.66	1,173.47	1,332.51
B1	0.5	0.089	0.074	0.051
	1.5	0.236	0.216	0.163
	2.0	0.360	0.261	0.211
	2.5	0.388	0.318	0.288
B2	0.5	0.147	0.124	0.080
	1.5	0.268	0.255	0.198
	2.0	0.386	0.321	0.236
	2.5	0.461	0.360	0.317
B3	0.5	0.147	0.124	0.080
	1.5	0.268	0.255	0.198
	2.0	0.386	0.321	0.236
	2.5	0.461	0.360	0.317
M1	0.8	0.069	0.092	0.167
	1.2	0.139	0.172	0.262
	2.3	0.337	0.290	0.368
	3.1	0.441	0.388	0.445
M2	0.7	0.158	0.148	0.234
	1.1	0.187	0.237	0.306
	2.2	0.404	0.361	0.437
	2.8	0.500	0.424	0.492
M3	0.7	0.346	0.230	0.150
	1.3	0.418	0.296	0.209
	1.7	0.488	0.349	0.266
	2.3	0.610	0.425	0.333
Q1	0.7	0.053	0.076	0.164
	1.3	0.170	0.164	0.241
	1.8	0.251	0.209	0.312
	2.4	0.333	0.294	0.362
Q2	0.73	0.196	0.232	0.101
	1.44	0.313	0.329	0.186
	2.15	0.407	0.403	0.259
	2.7	0.493	0.473	0.323
	0.9	0.031	0.097	0.236
Q3	1.3	0.099	0.146	0.305
	2.2	0.230	0.253	0.387
	2.7	0.307	0.313	0.448
Q4	0.7	0.076	0.080	0.059
	1.1	0.149	0.093	0.090
	1.5	0.185	0.158	0.121
	2.2	0.308	0.257	0.223
	2.3	0.327	0.243	0.233

(a)

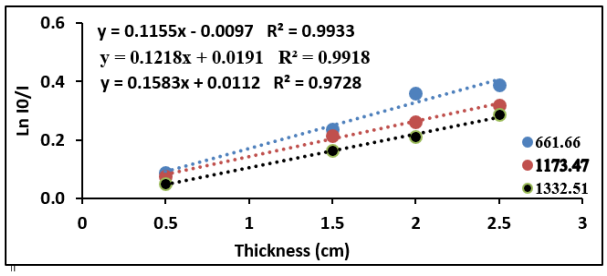

(b)

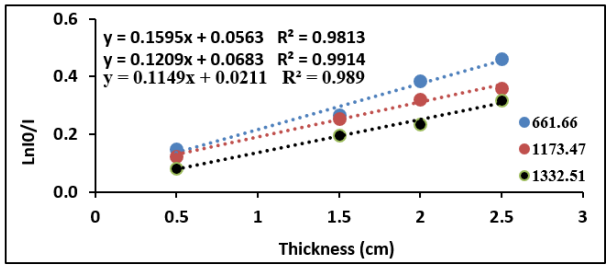

(c)

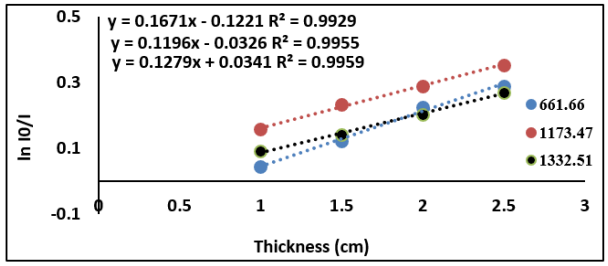

(d)

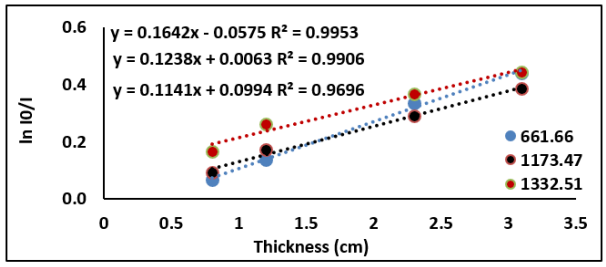

(e)

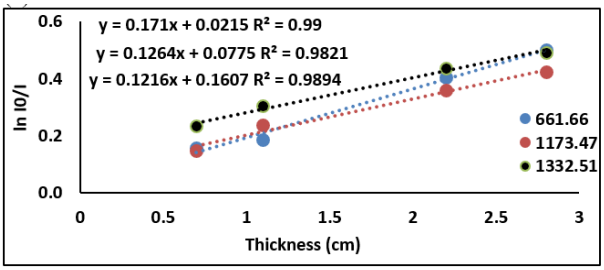

(f)

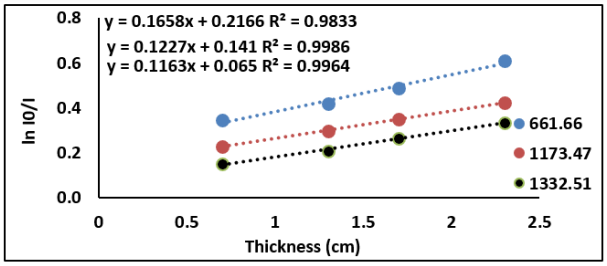

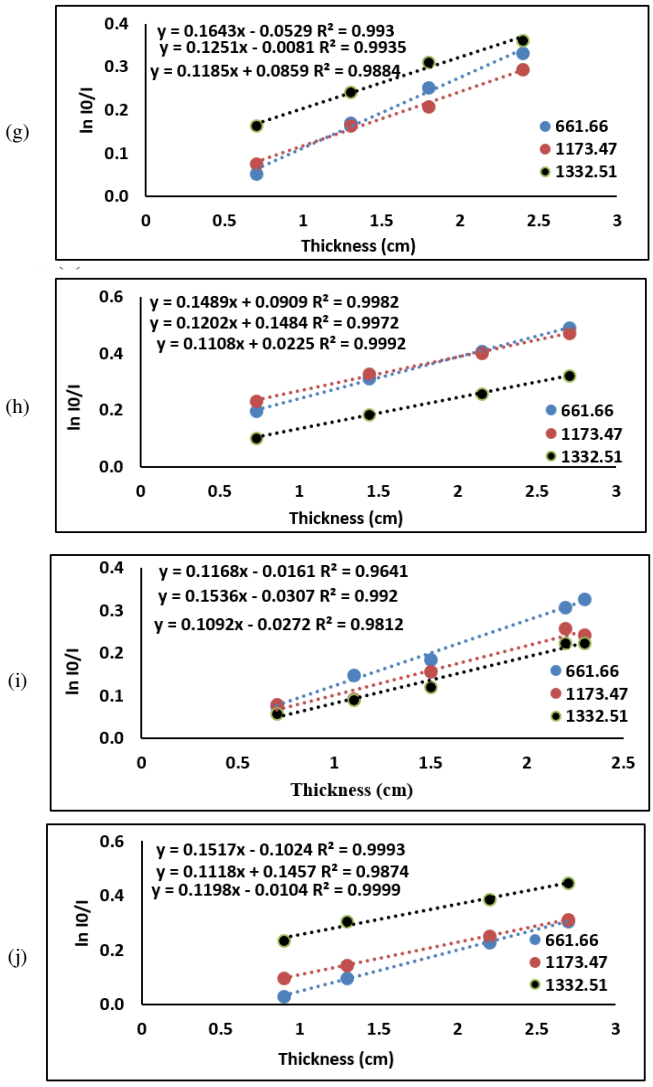

Fig. 3. Gamma transmission through (a) B1, (b) B2, (c) B3, (d) M1, (e) M2, (f) M3, (g) Q1, (h) Q2, (i) Q3, and (j) Q4 at different thicknesses and energies.

B. Mass Attenuation Coefficient

The density of bentonitic material in a dry state is contingent upon the quality of the material in question and may fluctuate between 2.2 g/cm³ and 2.8 g/cm³. The apparent density of bentonitic material when quarried and piled under natural moisture conditions has been observed to range from 1.5 g/cm³ to 1.8 g/cm³. The apparent density of milled bentonitic products is dependent upon the fineness of the milling process, with values ranging from 0.7 g/cm³ to 0.9 g/cm³. The variation of the mass attenuation coefficients for all bentonitic samples with incident photon energies is shown in Figure 5. At lower energies, where the photoelectric effect is dominant, the μ_m coefficients reach their maximum values and then exhibit an abrupt decline. This indicates that at low energies, the cross sections of gamma interactions with the electrons in the sample material exhibit an increase. Above 100 keV, all samples disclose a constrained range of μ_m coefficients and a less energy-dependent behavior. This is a direct consequence of the Compton Effect at these intermediate energies. The influence of the pair production process and the similarity in attenuation behavior for all photon energies beyond 10^{22} keV result in μ_m coefficients that are almost constant. As illustrated in Table IV, the mass attenuation coefficient increases with increasing density, and linear attenuation likewise increases.

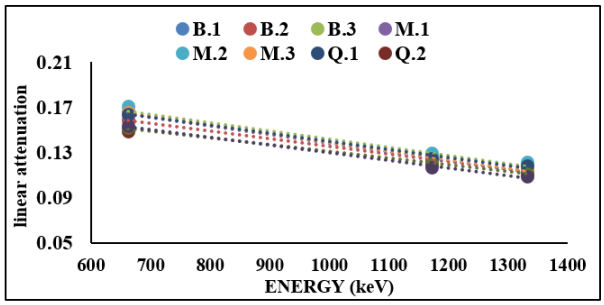

Fig. 4. Energy versus linear attenuation coefficient for various bentonitic material.

Theoretical or manual calculations using tabular data produced by a computer program may be considered as an alternative to a more practical approach than the experimental determination of mass attenuation coefficients. Authors in [31, 32] developed the computer software XCOM, which is capable of calculating the cross sections and attenuation coefficients for any given element, compound, or mixture at energies ranging from 1 keV to 100 GeV [33]. Theoretically, the mass attenuation coefficients (in cm²/g) of natural bentonitic were calculated implementing the XCOM program. A comparison of the predicted and experimental mass attenuation coefficients can be made using the XCOM computer program, as demonstrated in Table IV. It was established that there was a high level of correlation between the theoretical and experimental mass attenuation coefficients. The discrepancies between the experimental and theoretical data can be attributed to the disparate methodologies and databases employed by the various techniques, as well as the utilization of extended nuclear cross-section libraries. It is believed that the variations are not substantial, given that they fall within the reported experimental margin of error, which is 3.5% [34-37]. The mass attenuation coefficients were determined by comparing the experimental linear attenuation values for bentonite clay samples at various energies with other global values, as presented in Table V.

C. Effective Shield Thickness

One of the most crucial elements in the development of radiation shielding materials is the HVL. Consequently, an examination of the value of this kind of radiation allows for an analysis of the current materials' shielding capabilities. A reduction in the HVL results in enhanced shielding properties for the material in question. Consequently, the HVL value of the bentonitic shale sample showcases an inverse correlation with its shielding efficiency.

TABLE IV. THE DEVIATION BETWEEN THEORETICAL AND EXPERIMENTAL MASS ATTENUATION AT ENERGY OF 661.660 (KEV), 1,173.47 (KEV), AND 1,332.51 (KEV)

sample No.	ρ	661.660 (keV)				1,173.47 (keV)				1,332.51 (keV)			
		μ	μ_m (exp)	μ_m (theo)	Deviation (%)	μ	μ_m (exp)	μ_m (theo)	Deviation (%)	μ	μ_m (exp)	μ_m (theo)	Deviation (%)
B1	2.079	0.1583	0.0761	0.0773	1.51	0.1218	0.0586	0.0589	0.53	0.1155	0.0556	0.0552	0.61
B2	2.078	0.1595	0.0768	0.0774	0.81	0.1209	0.0582	0.0590	1.30	0.1149	0.0553	0.0553	0.06
B3	2.17	0.1671	0.0770	0.0771	0.18	0.1279	0.0589	0.0588	0.31	0.1195	0.0551	0.0551	0.04
Av.	2.109	0.1616	0.0766	0.0773	0.8333	0.1235	0.0586	0.0589	0.7133	0.1166	0.0553	0.0552	0.2367
M1	2.147	0.1642	0.0765	0.0767	0.22	0.1238	0.0577	0.0584	1.26	0.1141	0.0531	0.0548	2.93
M2	2.2	0.1710	0.0777	0.0775	0.36	0.1296	0.0589	0.059	0.15	0.1216	0.0553	0.0553	0.07
M3	2.125	0.1658	0.0780	0.0773	0.91	0.1227	0.0577	0.0589	1.98	0.1163	0.0547	0.0552	0.89
Av.	2.157	0.1670	0.0774	0.0772	0.4967	0.1254	0.0581	0.0588	1.1300	0.1173	0.0544	0.0551	1.2967
Q1	2.115	0.1643	0.0777	0.0770	0.91	0.1251	0.0591	0.0587	0.71	0.1185	0.0560	0.0550	1.91
Q2	1.985	0.1489	0.0750	0.0769	2.43	0.1202	0.0606	0.0586	3.39	0.1108	0.0558	0.0549	1.65
Q3	2.043	0.1517	0.0743	0.0772	3.78	0.1198	0.0586	0.0588	0.27	0.1118	0.0547	0.0551	0.72
Q4	2.004	0.1536	0.0766	0.0772	0.73	0.1168	0.0583	0.0588	0.91	0.1092	0.0545	0.0551	1.18
Av.	2.037	0.1546	0.0759	0.0771	1.9625	0.1205	0.0592	0.0587	1.3200	0.1126	0.0553	0.0550	1.3650

TABLE V. COMPARING THE MASS ATTENUATION COEFFICIENTS ($CM^2.G^{-1}$) OF THE TESTED SAMPLES AT THE INVESTIGATED GAMMA ENERGIES TO THOSE OF PRIOR RESEARCH CONDUCTED GLOBALLY

Sample Type	Energy (keV)			Country	References
	661.66	1,173.47	1,332.51		
B1	0.0761	0.0586	0.0556	Egypt	Present Work
B2	0.0768	0.0582	0.0553		
B3	0.0770	0.0589	0.0551		
M1	0.0765	0.0577	0.0531		
M2	0.0777	0.0589	0.0553		
M3	0.0780	0.0577	0.0547		
Q1	0.0777	0.0591	0.0560		
Q2	0.0750	0.0606	0.0558		
Q3	0.0743	0.0586	0.0547		
Q4	0.0766	0.0583	0.0545		
Worldwide					
Bentonite Clay	0.078	0.057	0.054	Egypt	[7]
bentonite–gypsum	0.0787	0.0586	0.0538	Egypt	[33].
Green marble	0.078	0.57	0.054	India	14]
Jet black granite	0.077	0.058	0.055		
Telephone black granite	0.077	0.058	0.054		
Cuddapah limestone	0.078.	0.058	0.055		
White marble	0.078	0.058	0.053		
Pink marble	0.078	0.058	0.055		
Olivine basalt	0.076	0.059	0.055		
Bentonite/PVA	0.076	0.059	0.056	Egypt	[15]
Natural bentonite	0.076	0.059	0.0543	Egypt	[20]
Pressed bentonite (50 bar)	0.0807	0.0615	0.0587		
Pressed bentonite (100 bar)	0.082	0.0626	0.0617		
Pressed bentonite (150 bar)	0.0857	0.0696	0.0652		
Barium–bismuth–borosilicate glasses	Range (0.072–0.084)	Range (0.053–0.057)	Range (0.050–0.052)	Iran	[32]
High consistency concrete	Range (0.08–0.078)	Range (0.053–0.057)	Range (0.053–0.054)	Turkey	[34]
Beige marble (KSA)	0.0756	0.0575	0.0552	KSA	[38]
Polyboron	0.087	0.066	0.062	Bangladesh	[39]
Ordinary concrete	0.078	0059	0.055		
Pure polyethylene	0.089	0.067	0.063		
Borated polyethylene	0.082	0.062	0.058		
Water	0.086	0.066	0.061		
Polymer (nylon 6)	0.086	0.065	0.061	India	[40]

TABLE VI. HVL, TVL, AND MFP FOR DIFFERENT BENTONITIC SHALE SAMPLES AT DIFFERENT ENERGIES

sample No.	HVL (cm)			TVL (cm)			MFP (cm)		
	661.660	1,173.47 (keV)	1,332.51	661.660	1,173.47 (keV)	1,332.51	661.660	1,173.47 (keV)	1,332.51
B1	4.378	5.690	6.000	14.529	18.883	19.913	6.3171	8.210	8.658
B2	4.345	5.732	6.031	14.420	19.024	20.017	6.2696	8.271	8.703
B3	4.147	5.418	5.800	13.764	17.983	19.247	5.984	7.819	8.368
M1	4.220	5.598	6.074	14.007	18.578	20.158	6.090	8.078	8.764

M2	4.053	5.347	5.6994	13.450	17.747	18.914	5.848	7.716	8.224
M3	4.180	5.648	5.9590	13.872	18.745	19.776	6.031	8.150	8.598
Q1	4.218	5.540	5.8489	13.999	18.385	19.409	6.086	7.994	8.439
Q2	4.654	5.765	6.2550	15.447	19.135	20.758	6.716	8.319	9.025
Q3	4.568	5.785	6.1990	15.162	19.199	20.572	6.592	8.347	8.945
Q4	4.512	5.933	6.3470	14.974	19.692	21.062	6.510	8.562	9.158

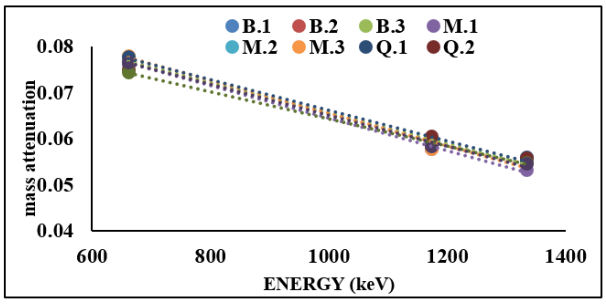

Fig. 5. Energy versus mass attenuation coefficient for various bentonitic materials.

Figure 6 provides a graphical representation of the energy dependency of the HVL values on photon energy. The necessity for thicker shields to safeguard against high gamma radiation is evident, given the consistent rise in HVL with photon energy. The observed changes in HVL values may be attributed to variations in the material's density. Furthermore, the HVL parameter can be employed to differentiate between samples based on their effectiveness in shielding. Accordingly, sample M2, comprising bentonite, exhibited the most effective shielding performance, accompanied by the lowest HVL at photon energies of 662, 1,173, and 1,332 keV. Conversely, sample Q2 demonstrated the lowest efficiency at 662 keV, while sample Q4 exhibited the lowest efficiency at 1,173 and 1,332 keV. The investigation revealed that the TVL and HVL values exhibited consistent behavior across different varieties of bentonitic shale, as shown in Table VI.

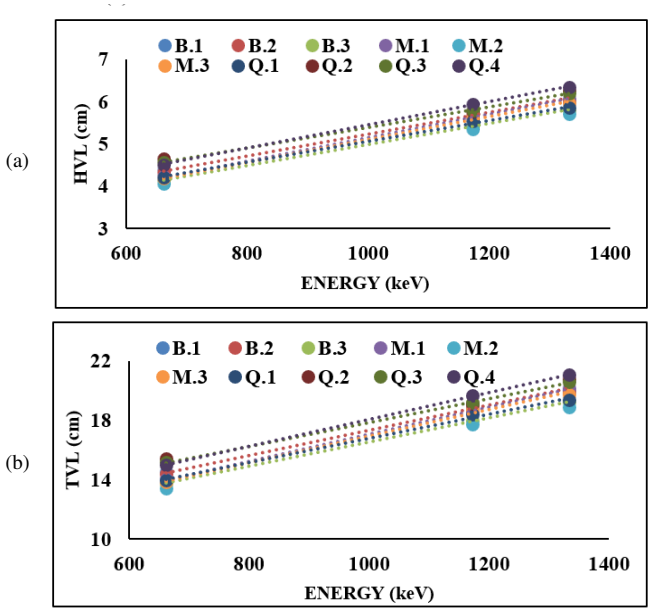

Fig. 6. Energy versus (a) HVL and (b) TVL for various bentonitic materials.

D. Mean Free Path

Table VI displays that the MFP for the M1, M2, and M3 samples from the Paleocene period exhibits the lowest values at 5.99cm, 7.98cm, and 8.529 cm, respectively, at energies of 661.66 keV, 1,173.47 keV, and 1,332.51 keV. Figure 7 demonstrates how the MFP values of the examined samples change with energy, exhibiting a diminishing sequence with increasing energy. The occurrence of gamma ray attenuation is indicated by the presence of low MFP values. The bentonitic sample M2, which has the maximum density (2.2 g/cm³), exhibits the lowest MFP values (5.848 cm, 7.716 cm, and 8.224 cm) at different energies, as illustrated in Table 6. All analyzed samples demonstrate an increase as gamma ray energy increases. This is due to the fact that a low energy photon can lose its energy in a shorter distance, while a high energy photon requires a longer distance.

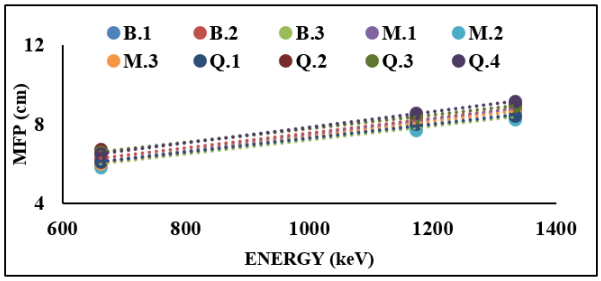

Fig. 7. Energy versus MFP for various bentonitic material.

V. CONCLUSIONS

Gamma radiation can be attenuated deploying a diverse array of materials. An understanding of the manner in which radiation attenuates as a result of physical interactions between photons and matter is beneficial in selecting an appropriate shielding material for a given application. As this understanding develops, it is essential to consider the physical, chemical, and economic limits in order to ensure the most effective use of resources in the development of appropriate shielding. The mass attenuation coefficient (μ_m) and the related parameters (HVL, TVL, and MFP) of the selected samples have been measured using a NaI(Tl) detector. Due to its wide availability and affordable price, bentonitic shale is a viable option for this use. The efficiency of nanoscale materials in gamma ray radiation has led to the natural occurrence of nanoscale bentonitic in volcanic ash deposits. The results indicated that:

- As thickness increases, the linear and mass attenuation coefficients also increase. The bentonitic samples B3 and M2 exhibit superior shielding parameters relative to other bentonitic samples, attributable to their elevated densities and extended periods.

- Given these characteristics, the Paleocene bentonitic sample M2 is the optimal material for this purpose, showcasing the highest linear attenuation coefficient and the least thickness (effective shielding).
- The experimental and theoretical values displayed a high degree of correlation, with the former and latter being in close agreement. Based on the HVL, TVL, and MFP values, bentonitic materials may be employed in radiation protection applications to shield individuals from the detrimental and hazardous effects of gamma radiation, given the prevalence of bentonitic shale globally and the toxicity of lead.
- Bentonitic materials from disparate sources (including those from Egypt and those reported by other researchers) manifest slight variations that may be attributed to differences in sample preparation or composition.
- This study makes a significant contribution to the field by providing an in-depth evaluation of natural bentonitic materials for gamma radiation shielding. It highlights the unique properties of these materials, which are attributed to their nanometer-scale structure and natural occurrence. The findings provide new insights into the effectiveness of bentonitic shales from specific geological periods, which may act as both efficient and cost-effective radiation protection solutions.

ACKNOWLEDGEMENTS

The authors extend their appreciation to Prince Sattam bin Abdulaziz University for funding this research work through the project number (PSAU/2023/01/24872).

REFERENCES

[1] F. Akman, Z. Y. Khattari, M. R. Kaçal, M. I. Sayyed, and F. Afaneh, "The radiation shielding features for some silicide, boride and oxide types ceramics," *Radiation Physics and Chemistry*, vol. 160, pp. 9–14, Jul. 2019, https://doi.org/10.1016/j.radphyschem.2019.03.001.

[2] F. Akman, M. R. Kaçal, M. I. Sayyed, and H. A. Karataş, "Study of gamma radiation attenuation properties of some selected ternary alloys," *Journal of Alloys and Compounds*, vol. 782, pp. 315–322, Apr. 2019, https://doi.org/10.1016/j.jallcom.2018.12.221.

[3] S. Asal, S. A. Erenturk, and S. Haciyakupoglu, "Bentonite based ceramic materials from a perspective of gamma-ray shielding: Preparation, characterization and performance evaluation," *Nuclear Engineering and Technology*, vol. 53, no. 5, pp. 1634–1641, May 2021, https://doi.org/10.1016/j.net.2020.11.009.

[4] Y. Q. Chen and B. H. Yan, "The technology of shielding design for nuclear reactor: A review," *Progress in Nuclear Energy*, vol. 161, Jul. 2023, Art. no. 104741, https://doi.org/10.1016/j.pnucene.2023.104741.

[5] G. Hu, H. Hu, Q. Yang, B. Yu, and W. Sun, "Study on the design and experimental verification of multilayer radiation shield against mixed neutrons and γ-rays," *Nuclear Engineering and Technology*, vol. 52, no. 1, pp. 178–184, Jan. 2020, https://doi.org/10.1016/j.net.2019.07.016.

[6] C. G. Hernandez-Murillo, J. R. Molina Contreras, L. A. Escalera-Velasco, H. A. de Leon-Martínez, J. A. Rodriguez-Rodriguez, and H. R. Vega-Carrillo, "X-ray and gamma ray shielding behavior of concrete blocks," *Nuclear Engineering and Technology*, vol. 52, no. 8, pp. 1792–1797, Aug. 2020, https://doi.org/10.1016/j.net.2020.01.007.

[7] M. Elsafi, Y. Koraim, M. Almurayshid, F. I. Almasoud, M. I. Sayyed, and I. H. Saleh, "Investigation of Photon Radiation Attenuation Capability of Different Clay Materials," *Materials*, vol. 14, no. 21, Jan. 2021, Art. no. 6702, https://doi.org/10.3390/ma14216702.

[8] K. Singh, N. Singh, and R. Kaundal, "Gamma-ray shielding and structural properties of PbO–SiO 2 glasses," *Nuclear Instruments and Methods in Physics Research Section B: Beam Interactions with Materials and Atoms*, vol. 266, pp. 944–948, Mar. 2008, https://doi.org/10.1016/j.nimb.2008.02.004.

[9] B. Ahmed, G. B. Shah, A. H. Malik, Aurangzeb, and M. Rizwan, "Gamma-ray shielding characteristics of flexible silicone tungsten composites," *Applied Radiation and Isotopes*, vol. 155, Jan. 2020, Art. no. 108901, https://doi.org/10.1016/j.apradiso.2019.108901.

[10] F. Cattant, D. Crusset, and D. Féron, "Corrosion issues in nuclear industry today," *Materials Today*, vol. 11, no. 10, pp. 32–37, Oct. 2008, https://doi.org/10.1016/S1369-7021(08)70205-0.

[11] B. Kanagaraj, N. Anand, A. Diana Andrushia, and M. Z. Naser, "Recent developments of radiation shielding concrete in nuclear and radioactive waste storage facilities – A state of the art review," *Construction and Building Materials*, vol. 404, Nov. 2023, Art. no. 133260, https://doi.org/10.1016/j.conbuildmat.2023.133260.

[12] A. Mansour, M. I. Sayyed, K. A. Mahmoud, E. Şakar, and E. G. Kovaleva, "Modified halloysite minerals for radiation shielding purposes," *Journal of Radiation Research and Applied Sciences*, vol. 13, no. 1, pp. 94–101, Jan. 2020, https://doi.org/10.1080/16878507.2019.1699680.

[13] M. I. Sayyed *et al.*, "Evaluation of gamma-ray and neutron shielding features of heavy metals doped Bi2O3-BaO-Na2O-MgO-B2O3 glass systems," *Progress in Nuclear Energy*, vol. 118, Jan. 2020, Art. no. 103118, https://doi.org/10.1016/j.pnucene.2019.103118.

[14] S. S. Obaid, M. I. Sayyed, D. K. Gaikwad, and Pravina. P. Pawar, "Attenuation coefficients and exposure buildup factor of some rocks for gamma ray shielding applications," *Radiation Physics and Chemistry*, vol. 148, pp. 86–94, Jul. 2018, https://doi.org/10.1016/j.radphyschem.2018.02.026.

[15] F. H. Sallam *et al.*, "Evaluation of gamma rays shielding competence for bentonite clay /PVA polymer matrix using MCNPX code," *Arab Journal of Nuclear Sciences and Applications*, vol. 53, no. 2, pp. 177–188, Apr. 2020, https://doi.org/10.21608/ajnsa.2020.18914.1292.

[16] M. B. Gili and F. Hila, "Investigation of Gamma-ray Shielding Features of Several Clay Materials Using the EPICS2017 Library," *Philippine Journal of Science*, vol. 150, pp. 1017–1026, Jul. 2021, https://doi.org/10.56899/150.05.13.

[17] F. H. Sallem, M. I. Sayyed, D. A. Aloraini, A. H. Almuqrin, and K. A. Mahmoud, "Characterization and Gamma-ray Shielding Performance of Calcinated and Ball-Milled Calcinated Bentonite Clay Nanoparticles," *Crystals*, vol. 12, no. 8, p. 1178, Aug. 2022, https://doi.org/10.3390/cryst12081178.

[18] N. Mesboua, K. Benyounes, and A. Benmounah, "Study of the impact of bentonite on the physico-mechanical and flow properties of cement grout," *Cogent Engineering*, vol. 5, no. 1, Jan. 2018, Art. no. 1446252, https://doi.org/10.1080/23311916.2018.1446252.

[19] A. Al-Reyahi, Y. Al-Degs, and A. Issa, "Assessment of Structure, Dielectric and Gamma-Shielding Properties of Chemically Treated Natural Kaolinite Clay," *Iranian Journal of Materials Science and Engineering*, vol. 18, no. 4, Aug. 2021, https://doi.org/10.22068/ijmse.2114.

[20] M. I. Abbas *et al.*, "Investigation of Gamma-Ray Shielding Properties of Bismuth Oxide Nanoparticles with a Bentonite–Gypsum Matrix," *Materials*, vol. 16, no. 5, Jan. 2023 Art. no. 2056, https://doi.org/10.3390/ma16052056.

[21] I. Z. Hager, Y. S. Rammah, H. A. Othman, E. M. Ibrahim, S. F. Hassan, and F. H. Sallam, "Nano-structured natural bentonite clay coated by polyvinyl alcohol polymer for gamma rays attenuation," *Journal of Theoretical and Applied Physics*, vol. 13, no. 2, pp. 141–153, Jun. 2019, https://doi.org/10.1007/s40094-019-0332-5.

[22] J. H. Hubbell, "Photon mass attenuation and energy-absorption coefficients," *The International Journal of Applied Radiation and Isotopes*, vol. 33, no. 11, pp. 1269–1290, Nov. 1982, https://doi.org/10.1016/0020-708X(82)90248-4.

[23] M. J. Berger *et al.*, *XCOM: Photon Cross Sections Database*. Gaithersburg, MD, USA: NIST, 2009.

[24] D. Degrelle, C. Mavon, and J.-E. Groetz, "Determination of mass attenuation coefficient by numerical absorption calibration with Monte-Carlo simulations at 59.54 keV," *Nuclear Instruments and Methods in Physics Research Section A: Accelerators, Spectrometers, Detectors and Associated Equipment*, vol. 816, pp. 47–52, Apr. 2016, https://doi.org/10.1016/j.nima.2016.01.075.

[25] B. O. El-bashir, M. I. Sayyed, M. H. M. Zaid, and K. A. Matori, "Comprehensive study on physical, elastic and shielding properties of ternary BaO-Bi2O3-P2O5 glasses as a potent radiation shielding material," *Journal of Non-Crystalline Solids*, vol. C, no. 468, pp. 92–99, 2017, https://doi.org/10.1016/j.jnoncrysol.2017.04.031.

[26] F. Sallam, E. Ibrahim, S. Hassan, and A. Omar, "Shielding Properties Enhancement of Bentonite Clay Nano Particles Coated by Polyvinyl Alcohol Polymer." Jun. 21, 2021, https://doi.org/10.21203/rs.3.rs-645961/v1.

[27] M. G. El-Samrah, A. F. Tawfic, F. H. Sallam, and A. M. Omar, "Investigation of specially designed bentonite samples as potential bricks with better radiation shielding properties," *Progress in Nuclear Energy*, vol. 162, Aug. 2023, Art. no. 104778, https://doi.org/10.1016/j.pnucene.2023.104778.

[28] L. Filipponi and D. Sutherland, *Introduction to nanoscience and nanotechnologies*. Denmark: Interdisciplinary Nanoscience Center (iNANO), 2011.

[29] F. Abdi, J. Derayat, R. Esmaeili, N. Fattahi, H. Sharafi, and A. Abdi, "X-ray transmission through nanostructured and microstructured tin oxide materials," vol. 8, pp. 18925–18933, Sep. 2016.

[30] M. M. Gouda, M. I. Abbas, S. I. Hammoury, K. Zard, and A. M. El-Khatib, "Nano tin oxide/dimethyl polysiloxane reinforced composite as a flexible radiation protecting material," *Scientific Reports*, vol. 13, no. 1, Jan. 2023, Art. no. 210, https://doi.org/10.1038/s41598-023-27464-z.

[31] M. J. Berger, J. H. Hubbell, S. M. Seltzer, J. S. Coursey, and D. S. Zucker, *XCOM: Photon Cross Section Database (version 1.2)*. Gaithersburg, MD, USA: NIST, 1999.

[32] H. S. Gökçe, B. C. Öztürk, N. F. Çam, and Ö. Andiç-Çakır, "Gamma-ray attenuation coefficients and transmission thickness of high consistency heavyweight concrete containing mineral admixture," *Cement and Concrete Composites*, vol. 92, pp. 56–69, Sep. 2018, https://doi.org/10.1016/j.cemconcomp.2018.05.015.

[33] M. Erdem, O. Baykara, M. Doğru, and F. Kuluöztürk, "A novel shielding material prepared from solid waste containing lead for gamma ray," *Radiation Physics and Chemistry*, vol. 79, no. 9, pp. 917–922, Sep. 2010, https://doi.org/10.1016/j.radphyschem.2010.04.009.

[34] R. Bagheri, A. K. Moghaddam, and H. Yousefnia, "Gamma Ray Shielding Study of Barium–Bismuth–Borosilicate Glasses as Transparent Shielding Materials using MCNP-4C Code, XCOM Program, and Available Experimental Data," *Nuclear Engineering and Technology*, vol. 49, no. 1, pp. 216–223, Feb. 2017, https://doi.org/10.1016/j.net.2016.08.013.

[35] H. Q. Vu, V. H. Tran, P. T. Nguyen, N. T. H. Le, and M. T. Le, "Radiation Shielding Properties Prediction of Barite used as Small Aggregate in Mortar," *Engineering, Technology & Applied Science Research*, vol. 10, no. 6, pp. 6469–6475, Dec. 2020, https://doi.org/10.48084/etasr.3880.

[36] S. David, M. Georgiou, E. Fysikopoulos, and G. Loudos, "Exprerimental Evaluation of a Dedicated Pinhole SPECT System for Small Animal Imaging and Scintimammography," *Engineering, Technology & Applied Science Research*, vol. 1, no. 1, pp. 17–22, Feb. 2011, https://doi.org/10.48084/etasr.9.

[37] M. R. Abdullah, O. K. Alghazawi, and M. Al-Ayyad, "Non-uniform Heat Source and Radiation Effect on a Transient MHD Flow Past a Vertical Moving Plate with Inclined Magnetic Field and Periodic Heat Flux," *Engineering, Technology & Applied Science Research*, vol. 9, no. 4, pp. 4361–4366, Aug. 2019, https://doi.org/10.48084/etasr.2779.

[38] I. F. Al-Hamarneh, "Investigation of gamma-ray shielding effectiveness of natural marble used for external wall cladding of buildings in Riyadh, Saudi Arabia," *Results in Physics*, vol. 7, pp. 1792–1798, Jan. 2017, https://doi.org/10.1016/j.rinp.2017.05.017.

[39] R. Biswas, H. Sahadath, A. S. Mollah, and Md. F. Huq, "Calculation of gamma-ray attenuation parameters for locally developed shielding material: Polyboron," *Journal of Radiation Research and Applied Sciences*, vol. 9, no. 1, pp. 26–34, Jan. 2016, https://doi.org/10.1016/j.jrras.2015.08.005.

[40] C. V. More, R. R. Bhosale, and P. P. Pawar, "Detection of new polymer materials as gamma-ray-shielding materials," *Radiation Effects and Defects in Solids*, vol. 172, no. 5–6, pp. 469–484, Jun. 2017, https://doi.org/10.1080/10420150.2017.1336765.